Available online at www.sciencedirect.com
ScienceDirect
Journal of Magnetic Resonance 186 (2007) 65–74
JMR Journal of Magnetic Resonance
www.elsevier.com/locate/jmr

Analytical theory of γ-encoded double-quantum recoupling sequences in solid-state nuclear magnetic resonance

Giuseppe Pileio, Maria Concistrè, Neville McLean, Axel Gansmüller, Richard C.D. Brown, Malcolm H. Levitt *

School of Chemistry, Southampton University, SO17 1BJ, UK

Received 8 November 2006; revised 9 January 2007
Available online 13 January 2007

Abstract

Many important double-quantum recoupling techniques in solid-state NMR are classified as being γ-encoded. This means that the phase of the double-quantum effective Hamiltonian, but not its amplitude, depends on the third Euler angle defining the orientation of the molecular spin system in the frame of the magic-angle-spinning rotor. In this paper, we provide closed analytical solutions for the dependence of the powder-average double-quantum-filtered signal on the recoupling times, within the average Hamiltonian approximation for γ-encoded pulse sequences. The validity of the analytical solutions is tested by numerical simulations. The internuclear distance in a $^{13}C_2$-labelled retinal is estimated by fitting the analytical curves to experimental double-quantum data.
© 2007 Elsevier Inc. All rights reserved.

Keywords: Recoupling; Symmetry-based recoupling; Magic-angle-spinning; Fresnel; Solid-state NMR

1. Introduction

Solid-state NMR is one of the most powerful experimental methods for addressing molecular structural problems, especially for insoluble or poorly crystalline systems. Many applications of solid-state NMR in polycrystalline or disordered materials employ a combination of methods: (i) magic-angle sample spinning [1,2] for improving resolution and sensitivity, (ii) cross-polarization [3,4] (CP) to enhance the NMR signals from weakly magnetic nuclear isotopes, and (iii) recoupling techniques [5–22] to reintroduce informative nuclear spin interactions which are averaged out by MAS.

Recoupling sequences employ radiofrequency pulse sequences which are synchronized with the sample rotation, in order to impede the averaging effect of the magic-angle-spinning on selected nuclear spin interactions. The through-space dipole–dipole coupling is usually the target of recoupling sequences, since this coupling encodes important geometric information through its dependence on the inverse cube of the internuclear distance [5–20]. The chemical shift anisotropy [21], or a combination of interactions [1,22] may also be recoupled. The design of recoupling pulse sequences is facilitated by the use of symmetry theory [7–20].

In most cases, the magnitude of a recoupled spin interaction depends on the relative orientation of the local molecular environment and the sample holder. It is convenient to discuss this dependence using the Euler angle triplet $\Omega_{MR} = \{\alpha_{MR}, \beta_{MR}, \gamma_{MR}\}$ which defines the relative orientation of a reference frame M which is fixed with respect to the molecular framework, and a reference frame R fixed with respect to the rotating sample holder. The z-axis of frame R is defined to be along the sample rotation axis. In a disordered sample, the three Euler angles $\Omega_{MR} = \{\alpha_{MR}, \beta_{MR}, \gamma_{MR}\}$ are random, isotropically distributed variables. This paper uses the notation and conventions for Euler angles and reference frames given in Ref. [11].

In general, a recoupling sequence leads to a first-order average Hamiltonian for a recoupled interaction Λ of the following form:

* Corresponding author. Fax: +44 23 8059 3781.
E-mail address: mhl@soton.ac.uk (M.H. Levitt).

1090-7807/$ - see front matter © 2007 Elsevier Inc. All rights reserved.
doi:10.1016/j.jmr.2007.01.009

$$\overline{\mathcal{H}}_{\Lambda}^{(1)} = \omega_{\lambda\mu}^{\Lambda}(\Omega_{\mathrm{MR}})T_{\lambda\mu}^{\Lambda} + \omega_{\lambda\mu}^{\Lambda}(\Omega_{\mathrm{MR}})^{*}T_{\lambda-\mu}^{\Lambda} \quad (1)$$

where $T_{\lambda\mu}^{\Lambda}$ is a spherical tensor operator of rank λ and component index μ, defined with respect to rotations of the resonant nuclear spins. The rank λ and component index μ depend on the nature of the recoupling pulse sequence. For example, double-quantum dipolar recoupling [5–9,17,18] has $\lambda = 2$ and $\mu = 2$; zero-quantum homonuclear dipolar recoupling [13,15] has $\lambda = 2$ and $\mu = 0$. Heteronuclear dipolar recoupling of the REDOR type [23,24] has $\lambda = 1$ and $\mu = 0$.

The amplitude of the recoupled interaction is given by the complex number $\omega_{\lambda}^{\Lambda}\mu(\Omega_{\mathrm{MR}})$, which depends on the orientation Ω_{MR}. The form of this orientation-dependence also depends on the recoupling sequence. In general, both the magnitude and the phase of the amplitude $\omega_{\lambda\mu}^{\Lambda}$ depends on any combination of the three angles $\Omega_{\mathrm{MR}} = \{\alpha_{\mathrm{MR}}, \beta_{\mathrm{MR}}, \gamma_{\mathrm{MR}}\}$. However, for an important class of recoupling sequences, the recoupling amplitude has the form:

$$\omega_{\lambda\mu}^{\Lambda}(\Omega_{\mathrm{MR}}) = |\omega_{\lambda\mu}^{\Lambda}(\alpha_{\mathrm{MR}}, \beta_{\mathrm{MR}})|\mathrm{e}^{\mathrm{i}\phi_{\lambda\mu}^{\Lambda}(\gamma_{\mathrm{MR}})} \quad (2)$$

where the phase angle $\phi_{\lambda\mu}^{\Lambda}$ is a function of the single Euler angle γ_{MR}, while the magnitude $|\omega_{\lambda\mu}^{\Lambda}|$ is independent of γ_{MR}. Pulse sequences which generate average Hamiltonians obeying Eq. (2) are termed γ-*encoded* [6]. Examples of γ-encoded recoupling phenomena include rotational resonance [25,26], homonuclear rotary resonance (HORROR) [6], and a range of symmetry-based recoupling sequences [7–20], including C7 [7] and POST-C7 [8]. Recoupling sequences which are *not* γ-encoded include REDOR [23,24], TEDOR [27], DRAMA [5], RFDR [28], and some supercycled symmetry-based recoupling sequences such as SR26 [17].

The attribute of γ-encoding provides both advantages and disadvantages. In general, the reduced orientation-dependence of γ-encoded pulse sequences leads to stronger oscillations of the NMR signal as a function of the recoupling interval, which allows a more accurate determination of the recoupled interaction magnitude. In the case of double-quantum recoupling, the maximum achievable double-quantum-filtering efficiency in powder samples is significantly higher for γ-encoded sequences than for non-γ-encoded sequences. In addition, γ-encoded sequences allow a finer time-resolution of the recoupling intervals compared to non-γ-encoded sequences [20]. On the other hand, γ-encoded sequences tend to be less robust at long times compared to non-γ-encoded sequences [17].

The orientation-dependence of the recoupling sequence leads to an orientation-dependent NMR signal. Consider an NMR experiment involving a recoupling sequence of duration τ. The powder-average NMR signal is an orientational average of the form:

$$\langle s(\tau)\rangle = (8\pi^2)^{-1}\int_0^{2\pi} \mathrm{d}\alpha_{\mathrm{MR}} \int_0^{\pi} \mathrm{d}\beta_{\mathrm{MR}} \int_0^{2\pi} \mathrm{d}\gamma_{\mathrm{MR}} \sin\beta_{\mathrm{MR}} s(\tau, \Omega_{\mathrm{MR}}) \quad (3)$$

where the form of $s(\tau,\Omega_{\mathrm{MR}})$ depends on the recoupling sequence, the orientational angles Ω_{MR}, and the experimental protocol, as discussed below. Average Hamiltonian theory often provides a closed analytical expression for the signal from a given molecular orientation, $s(\tau,\Omega_{\mathrm{MR}})$, under suitable approximations. In some cases, closed analytical expressions are also available for the powder average signal in Eq. (3). Such analytical solutions are very useful for molecular structural studies since they allow a rapid fitting of the experimental data to structural constraints. For example, analytical formulae based on quarter-integer-order Bessel functions were derived by Mueller for the case of the REDOR dephasing curve [29–31]. Similar functions were derived for the case of the non-γ-encoded supercycled SR26 sequence [17]. These analytical solutions were essential for the structure determination of network solids by double-quantum ^{29}Si NMR, since in that case many thousands of structural models were tested by comparison of theory and experiment [32,33].

In the case of pulse sequences including REDOR [23,24] and SR26 [17], which are not γ-encoded, a suitable choice of reference frame reduces the triple integral in Eq. (3) to a double integral over the angles β_{MR} and γ_{MR}. As shown by Mueller [29–31], this double integral may be expressed as a closed expression involving quarter-integer-order Bessel functions. The analytical expressions may be evaluated very rapidly, allowing the rapid fitting of molecular structure parameters.

In the case of γ-encoded sequences such as C7 [7], under the specific experimental protocols discussed below, the powder-average double-quantum-filtered NMR signal may be reduced to a *single* integral over the angle β_{MR}. Although this single integral is superficially simpler than the double integral required for non-γ-encoded sequences, a closed analytical form for the powder average γ-encoded signal has not been available, although an expression involving an infinite Bessel series has been reported [29]. The lack of a closed analytical form has impeded the application of γ-encoded recoupling sequences in iterative molecular structure determination protocols.

In this paper, we provide closed solutions for powder-average γ-encoded NMR signals in terms of Fresnel functions. We compare the Fresnel solutions with numerical simulations, examining the effect of chemical shift anisotropy and rf inhomogeneity in typical experimental regimes. We show that the analytical solutions may be used to extract molecular structure information rapidly and reliably from experimental double-quantum ^{13}C data.

2. Pulse sequences

2.1. Symmetry-based recoupling

The principles of symmetry-based recoupling sequences have been described in many other places [7–20] and need only be summarized briefly here. There are two major classes of symmetry-based recoupling sequence, denoted CN_n^{ν}

and RN_n^ν. A pulse sequence with the symmetry CN_n^ν or RN_n^ν is composed of N elements $\{\varepsilon_0\varepsilon_1\ldots\ \varepsilon_{N-1}\}$, each of which has the same duration $\tau_E = n\tau_r/N$, where τ_r is a period of the magic-angle sample rotation, $\tau_r = |2\pi/\omega_r$, and the angular spinning frequency is ω_r. In the case of CN_n^ν sequences [7–13], the elements are derived from a basic element $\mathcal{C}^0$ by an incremental phase shift:

$$\varepsilon_q = \mathcal{C}^0_{2\pi q\nu/N} \tag{4}$$

In the case of RN_n^ν sequences [14–19], the phases alternate between two values:

$$\varepsilon_q = \begin{cases} \mathcal{R}^0_{\pi\nu/N} & (q \text{ even}) \\ \mathcal{R}^{0\prime}_{-\pi\nu/N} & (q \text{ odd}) \end{cases}$$

where the prime indicates that all phases internal to the basic element $\mathcal{R}^0$ are changed in sign, and a subscript indicates an overall phase shift. Sequences with the symmetry CN_n^ν are based on an element $\mathcal{C}^0$ which must be a *rf cycle* (propagator proportional to the identity operator); sequences with the symmetry RN_n^ν are based on an *inversion element* $\mathcal{R}^0$ which provides a rotation through an odd multiple of π about the rotating-frame x-axis.

The integers N, n and ν are called *symmetry numbers* and control the recoupling properties of the pulse sequence through the following *selection rules* on the first-order average Hamiltonian:

$$\overline{\mathcal{H}}^{(1)}_{\ell m\lambda\mu}(CN_n^\nu) = 0 \quad \text{if } mn - \mu\nu \neq N \tag{5}$$

and

$$\overline{\mathcal{H}}^{(1)}_{\ell m\lambda\mu}(RN_n^\nu) = 0 \quad \text{if } mn - \mu\nu \neq \tfrac{1}{2}NZ_\lambda \tag{6}$$

where Z_λ is an integer with the same parity as λ. The quantum numbers $\{\ell, m, \lambda, \mu\}$ characterize the rotational properties of an individual spin interaction term: the "space" rotational properties are characterized by a rank ℓ and component index $m \in \{-\ell, -\ell+1, \ldots, \ell\}$. The "spin" rotational properties are characterized by a rank λ and component $\mu \in \{-\lambda, -\lambda+1, \ldots, \lambda\}$. The various nuclear spin interactions are distinguished by the values of ℓ and λ: For homonuclear dipole–dipole interactions, $\{\ell, \lambda\} = \{2, 2\}$; for isotropic chemical shifts, $\{\ell, \lambda\} = \{0, 1\}$; for chemical shift anisotropies, $\{\ell, \lambda\} = \{2, 1\}$. The selection rules Eqs. (5) and (6) may be used to select the appropriate symmetry class (CN_n^ν or RN_n^ν) and symmetry numbers $\{N, n, \nu\}$ for a given recoupling task.

2.2. γ-Encoded double-quantum recoupling

In this article, we are mainly concerned with γ-encoded homonuclear double-quantum recoupling sequences, which have the following properties:

1. All terms $\overline{\mathcal{H}}^{(1)}_{\ell m\lambda\mu}$ with $\mu \neq \pm 2$ vanish;
2. There is only one symmetry-allowed term of the form $\overline{\mathcal{H}}^{(1)}_{2m22}$, and only one symmetry-allowed term of the form $\overline{\mathcal{H}}^{(1)}_{2m2-2}$.

The latter condition ensures a one-to-one correspondence between the symmetry-allowed spin and spatial components, which is the essence of γ-encoding. There are therefore four types of γ-encoded double-quantum recoupling sequences:

1. Sequences providing symmetry-allowed terms of the form $\overline{\mathcal{H}}^{(1)}_{2\pm12\pm2}$.
2. Sequences providing symmetry-allowed terms of the form $\overline{\mathcal{H}}^{(1)}_{2\pm12\mp2}$.
3. Sequences providing symmetry-allowed terms of the form $\overline{\mathcal{H}}^{(1)}_{2\pm22\pm2}$.
4. Sequences providing symmetry-allowed terms of the form $\overline{\mathcal{H}}^{(1)}_{2\pm22\mp2}$.

The first and second types are called $m = 1$ *double-quantum recoupling sequences*. The third and fourth types are called $m = 2$ *double-quantum recoupling sequences*.

Tables of symmetry numbers for implementing the two main classes of γ-encoded double-quantum recoupling are provided in ref.20. Examples of $m = 1$ double-quantum recoupling symmetries are $C7_2^1$, $R14_2^6$, $R20_2^9$ and $R26_4^{11}$ [7,14,16–18]. Examples of $m = 2$ double-quantum recoupling symmetries are $C8_1^3$ and $C8_3^1$ [20].

2.3. Double-quantum filtering

A typical radiofrequency pulse sequence, suitable for the ^{13}C spectroscopy of ^{13}C-labelled organic materials, is shown in Fig. 1.

A ramped cross-polarization (CP) block [34] is used to enhance the transverse magnetization of the S-spin species (usually ^{13}C). A π/2 pulse, phase-shifted by π/2, rotates the ^{13}C transverse magnetization to the longitudinal direction. A double-quantum recoupling sequence is applied for an interval τ_{exc} in order to transform the enhanced longitudinal magnetization into double-quantum coherence. A second recoupling sequence of duration τ_{rec}, followed by another π/2 pulse, transforms the

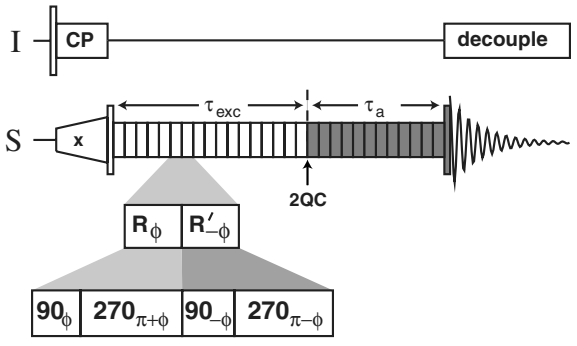

Fig. 1. Double-quantum recoupling pulse sequence for a rare spin species S, including cross-polarization from an abundant spin species I. The shaded pulse sequence elements are given a phase cycle in order to select S-spin signals passing through double-quantum coherences at the indicated time point. The figure illustrates the implementation of a RN_n^ν pulse sequence based on a broadband $\mathcal{R}^0$ element.

double-quantum coherence into observable transverse magnetization. In suitable cases, the heteronuclear decoupler field may be turned off during the double-quantum recoupling intervals [12,19]. Standard phase-cycling [35] of the shaded pulse sequence elements is used to suppress NMR signals that did not pass through double-quantum coherence at the end of the interval τ_{exc}. This is called double-quantum filtering (DQF).

The dipole–dipole coupling between nuclear spins may be estimated by acquiring double-quantum-filtered NMR signals as a function of the intervals τ_{exc} and τ_{rec}. Two protocols are commonly used [16]: in the *symmetric* protocol, the two intervals τ_{exc} and τ_{rec} are both incremented but kept equal to each other. In the *asymmetric* protocol, one of the two intervals is kept fixed (usually τ_{rec}) while the other is incremented. The asymmetric protocol leads to higher dynamic range in the dipolar oscillations, while the symmetric protocol does not require a prior estimate of the dipole–dipole coupling constant [16].

3. Theory

3.1. Average Hamiltonian

The average Hamiltonian theory [36] of symmetry-based double-quantum recoupling sequences leads to the following first-order average Hamiltonian, for the case of isolated pairs of spins-1/2, I_j and I_k:

$$\overline{\mathcal{H}}^{(1)}(\Omega_{MR},t^0)=\omega_{jk}(\Omega_{MR},t^0)T^{jk}_{2,2}+\omega^*_{jk}(\Omega_{MR},t^0)T^{jk}_{2,-2}+2\pi J_{jk}\mathbf{I}_j\cdot\mathbf{I}_k \tag{7}$$

where the spherical tensor operators are given by $T^{jk}_{2,\pm2}=\frac{1}{2}I^{\pm}_jI^{\pm}_k$. Here t^0 is the time point at which the recoupling sequence is initiated and J_{jk} is the scalar coupling constant between j and k.

For simplicity, we choose the molecular reference frame M to coincide with the principal axis frame of the I_j-I_k dipole–dipole interaction. For a γ-encoded recoupling sequence, the symmetry-allowed average Hamiltonian terms have quantum numbers $\{\ell,m,\lambda,\mu\}=\{2,\pm m,2,\pm2\}$, where the value of m depends on the pulse sequence symmetry (for $C7^1_2m=+1$, while for $R14^6_2$, $R20^9_2$, $R26^{11}_4$, etc., $m=-1$). In general, the recoupled double-quantum dipole–dipole interaction has the following amplitude:

$$\begin{aligned}\omega_{jk}(\Omega_{MR},t^0)&=\sqrt{6}b_{jk}\kappa_{2m22}D^2_{0m}(\Omega_{MR})e^{-im(\alpha^0_{RL}-\omega_rt^0)}\\&=\sqrt{6}b_{jk}\kappa_{2m22}d^2_{0m}(\beta_{MR})e^{-im(\gamma_{MR}+\alpha^0_{RL}-\omega_rt^0)}\end{aligned} \tag{8}$$

where $d^2_{0m}(\beta_{MR})$ is a reduced Wigner matrix element, and κ_{2m22} is the scaling factor for the recoupled term, which depends on the details of the basic element. The dipole–dipole coupling constant is given by $b_{jk}=-(\mu_0/4\pi)\gamma^2\hbar r^{-3}_{jk}$ where r_{jk} is the internuclear distance, neglecting molecular motion. Eq. (8) contains the essential properties of γ-encoding (the phase, but not the amplitude, of ω_{jk} depends on the angle γ_{MR}).

3.2. Double-quantum-filtered signal

The double-quantum-filtered signal amplitude for the pulse sequence in Fig. 1 is given by

$$f_{DQ}(\tau_{exc},\tau_{rec})=f_{+2}(\tau_{exc},\tau_{rec})+f_{-2}(\tau_{exc},\tau_{rec}) \tag{9}$$

with:

$$f_{\pm2}(\tau_{exc},\tau_{rec})=(I_zI_z)^{-2}\langle(I_z|U_{rec}I^{\pm}_jI^{\pm}_kU^{\dagger}_{rec})(I^{\pm}_jI^{\pm}_k|U_{exc}I_zU^{\dagger}_{exc})\rangle \tag{10}$$

where the total longitudinal angular momentum operator is $I_z=I_{jz}+I_{kz}$ and the scalar product in operator space [37] is defined by $(A|B)=\mathrm{Tr}\{A^{\dagger}B\}$. The angular brackets denote an average over all molecular orientations. The propagators for the excitation and reconversion sequences are given by

$$\begin{aligned}U_{exc}&\approx\exp\{-i\Phi_{exc}I_z\}\exp\{-i\overline{\mathcal{H}}^{(1)}(\Omega_{MR},t^0_{exc})\tau_{exc}\}\exp\{+i\Phi_{exc}I_z\}\\U_{rec}&\approx\exp\{-i\Phi_{rec}I_z\}\exp\{-i\overline{\mathcal{H}}^{(1)}(\Omega_{MR},t^0_{rec})\tau_{rec}\}\exp\{+i\Phi_{rec}I_z\}\end{aligned} \tag{11}$$

where $\{t^0_{exc},t^0_{rec}\}$ are the starting time points of the excitation and reconversion sequences, and $\{\Phi_{exc},\Phi_{rec}\}$ are the overall radiofrequency phases.

In the case of CN^{ν}_n sequences, the timings and the phases are correlated with each other so that [20]

$$m\omega_rt^0_{exc}-2\Phi_{exc}+\pi=m\omega_rt^0_{rec}-2\Phi_{rec}\quad\text{for } CN^{\nu}_n \text{ sequences} \tag{12}$$

In the case of RN^{ν}_n sequences, a simpler relationship applies:

$$-2\Phi_{exc}+\pi=-2\Phi_{rec}\quad\text{for } RN^{\nu}_n \text{ sequences} \tag{13}$$

These phase-time relationships ensure compatible double-quantum excitation and reconversion processes, even for incomplete recoupling cycles. This property allows a fine time-resolution of the excitation and reconversion sequences, which is one of the special advantages of γ-encoded sequences [20]. If the phase-time relationships are satisfied, Eq. (10) may be written:

$$\begin{aligned}f_{\pm2}(\tau_{exc},\tau_{rec})=&-(I_zI_z)^{-2}\langle(I_z|U^0_{rec}I^{\pm}_jI^{\pm}_kU^{0\dagger}_{rec})\\&\times(I^{\pm}_jI^{\pm}_k|U^0_{exc}I_zU^{0\dagger}_{exc})\rangle\end{aligned} \tag{14}$$

where

$$\begin{aligned}U^0_{exc}&\approx\exp\{-i\overline{\mathcal{H}}^{(1)}(\Omega_{MR},t^0)\tau_{exc}\}\\U^0_{rec}&\approx\exp\{-i\overline{\mathcal{H}}^{(1)}(\Omega_{MR},t^0)\tau_{rec}\}\end{aligned} \tag{15}$$

and t^0 is a common time origin for the entire pulse sequence.

Define a set of three double-quantum operators as follows:

$$I_x^{DQ} = \tfrac{1}{2}(I_j^+ I_k^+ + I_j^+ I_k^-)$$
$$I_y^{DQ} = \tfrac{1}{2i}(I_j^+ I_k^+ - I_j^+ I_k^-)$$
$$I_z^{DQ} = \tfrac{1}{2} I_z \quad (16)$$

These operators cyclically commute:

$$[I_x^{DQ}, I_y^{DQ}] = i I_z^{DQ} \quad \text{(cyclic)} \quad (17)$$

The average Hamiltonian in Eq. (7) may be written:

$$\overline{\mathcal{H}}^{(1)}(\Omega_{MR}, t^0) = |\omega_{jk}(\beta_{MR})| \exp\{-i\phi_{DQ} I_z^{DQ}\} I_x^{DQ} \times \exp\{+i\phi_{DQ} I_z^{DQ}\} + 2\pi J_{jk} \mathbf{I}_j \cdot \mathbf{I}_k \quad (18)$$

where the complex amplitude of the recoupled double-quantum interaction is given by

$$\omega_{jk}(\beta_{MR}) = |\omega_{jk}(\beta_{MR})| \exp\{-i\phi_{DQ}\} \quad (19)$$

and the phase angle is given by

$$\phi_{DQ} = \arg\{\kappa_{2m22}\} - m\gamma_{MR} - m\alpha_{RL}^0 + m\omega_r t^0 \quad (20)$$

This conforms to the γ-encoding property in Eq. (2). Since the double-quantum operators commute with the J-coupling term, the transformation of z-angular momentum by the excitation sequence is given by

$$U(\tau_{exc}) I_z^{DQ} U(\tau_{exc}) = \cos(|\omega_{jk}|\tau_{exc}) I_z^{DQ} + \sin(|\omega_{jk}|\tau_{exc}) \exp\{-i\phi_{DQ} I_z^{DQ}\} I_y^{DQ} \exp\{+i\phi_{DQ} I_z^{DQ}\} \quad (21)$$

and hence

$$(I_j^\pm I_k^\pm | U_{exc}^0 I_z U_{exc}^{0\dagger}) = \mp i \sin(|\omega_{jk}|\tau_{exc}) \exp\{\mp i\phi_{DQ}\} \quad (22)$$

Similarly,

$$(I_z | U_{rec}^0 I_j^\pm I_k^\pm U_{rec}^{0\dagger}) = \pm i \sin(|\omega_{jk}|\tau_{exc}) \exp\{\pm i\phi_{DQ}\} \quad (23)$$

The powder-average double-quantum-filtering efficiency is therefore given by

$$f_{DQ}(\tau_{exc}, \tau_{rec}) \cong \langle \sin(|\omega_{jk}|\tau_{exc}) \sin(|\omega_{jk}|\tau_{rec}) \rangle \quad (24)$$

This signal is dependent on the value of m for the recoupled double-quantum term. The expressions for the relevant Wigner matrix elements are:

$$d^2_{0,\pm2}(\beta) = \sqrt{\frac{3}{8}} \sin^2\beta$$
$$d^2_{0,\pm1}(\beta) = \pm\sqrt{\frac{3}{8}} \sin 2\beta \quad (25)$$

The double-quantum-filtered signal amplitude may therefore be written:

$$f_{DQ}(\tau_{exc}, \tau_{rec}) \cong F_{DQ}(\theta_{exc}, \theta_{rec}) \quad (26)$$

where the angles θ_{exc} and θ_{rec} are defined by

$$\theta_{exc} = \tfrac{3}{2}|\kappa_{2m22}| b_{jk} \tau_{exc}$$
$$\theta_{rec} = \tfrac{3}{2}|\kappa_{2m22}| b_{jk} \tau_{rec} \quad (27)$$

and the function F_{DQ} is given by:

$$F_{DQ}(\theta_{exc}, \theta_{rec}) = \begin{cases} \langle \sin(\theta_{exc} \sin(2\beta_{MR})) \sin(\theta_{rec} \sin(2\beta_{MR})) \rangle & \text{for } m = \pm 1 \\ \langle \sin(\theta_{exc} \sin^2\beta_{MR}) \sin(\theta_{rec} \sin^2\beta_{MR}) \rangle & \text{for } m = \pm 2 \end{cases} \quad (28)$$

The function F_{DQ} has a "universal" form, which is independent of the dipole–dipole coupling and the pulse sequence scaling factor.

Since the double-quantum-filtered signal is independent of the angles α_{MR} and γ_{MR}, the orientational averages in Eq. (28) may be written in terms of single integrals over β_{MR}:

$$F_{DQ}(\theta_{exc}, \theta_{rec}) = \begin{cases} \frac{1}{2}\int_0^\pi d\beta_{MR} \sin\beta_{MR} \sin(\theta_{exc} \sin(2\beta_{MR})) \sin(\theta_{rec} \sin(2\beta_{MR})) & \text{for } m = \pm 1 \\ \frac{1}{2}\int_0^\pi d\beta_{MR} \sin\beta_{MR} \sin(\theta_{exc} \sin^2\beta_{MR}) \sin(\theta_{rec} \sin^2\beta_{MR}) & \text{for } m = \pm 2 \end{cases} \quad (29)$$

4. Analytical solutions

Special cases of Eq. (29) have been solved by Mueller et al. [29–31], using Bessel functions [38]. However, the solutions achieved were not in a closed form. Here, we report closed-form solutions in terms of Fresnel functions [39], obtained with the help of Mathematica version 5.2 [40].

After several manual substitutions of variables, Mathematica finds the following solution for Eq. (29):

$$F_{DQ}(\theta_{exc}, \theta_{rec}) = \frac{1}{2x_\Delta}(F_c(x_\Delta)\cos(\theta_\Delta) + F_s(x_\Delta)\sin(\theta_\Delta)) - \frac{1}{2x_\Sigma}(F_c(x_\Sigma)\cos(\theta_\Sigma) + F_s(x_\Sigma)\sin(\theta_\Sigma)) \quad (30)$$

where

$$\theta_\Delta = \theta_{exc} - \theta_{rec}$$
$$\theta_\Sigma = \theta_{exc} + \theta_{rec} \quad (31)$$

and

$$x_\Delta = \left\{\frac{2\theta_\Delta}{\pi}\right\}^{1/2}$$
$$x_\Sigma = \left\{\frac{2\theta_\Sigma}{\pi}\right\}^{1/2} \quad (32)$$

Here $F_c(x)$ is the Fresnel cosine integral [39], given by:

$$F_c(x) = \int_0^x \cos\left(\frac{\pi y^2}{2}\right) dy \quad (33)$$

while $F_s(x)$ is the Fresnel sine integral, given by:

$$F_s(x) = \int_0^x \sin\left(\frac{\pi y^2}{2}\right) dy \quad (34)$$

The expressions in Eq. (30) resemble those given many years ago by Look et al., for the free-induction-decay

generated by randomly oriented spin-1/2 pairs in a static solid [41].

Surprisingly, the analytical solution of Eq. (30) is exactly the same for $m = \pm 1$ and $m = \pm 2$ double-quantum recoupling, corresponding to the two versions of the double-quantum-filtered signal given in Eq. (29). So far, a deeper reason for the identity of these two results has not been discovered.

A contour plot of the function $F_{\mathrm{DQ}}(\theta_{\mathrm{exc}}, \theta_{\mathrm{rec}})$ against the excitation and reconversion time variables is shown in Fig. 2a. This shows characteristic strong oscillations which may be used to determine the dipole–dipole coupling constant. The highest amplitudes are observed along the diagonal ($\theta_{\mathrm{exc}} = \theta_{\mathrm{rec}}$), with a global maximum of 0.733 at $\theta_{\mathrm{exc}} = \theta_{\mathrm{rec}} = 0.\ 602\pi$. Strong negative double-quantum-filtered amplitudes are observed off the diagonal. The global minimum is -0.398 which is found at $\{\theta_{\mathrm{exc}}, \theta_{\mathrm{rec}}\} = \{0.513\pi, 1.716\pi\}$.

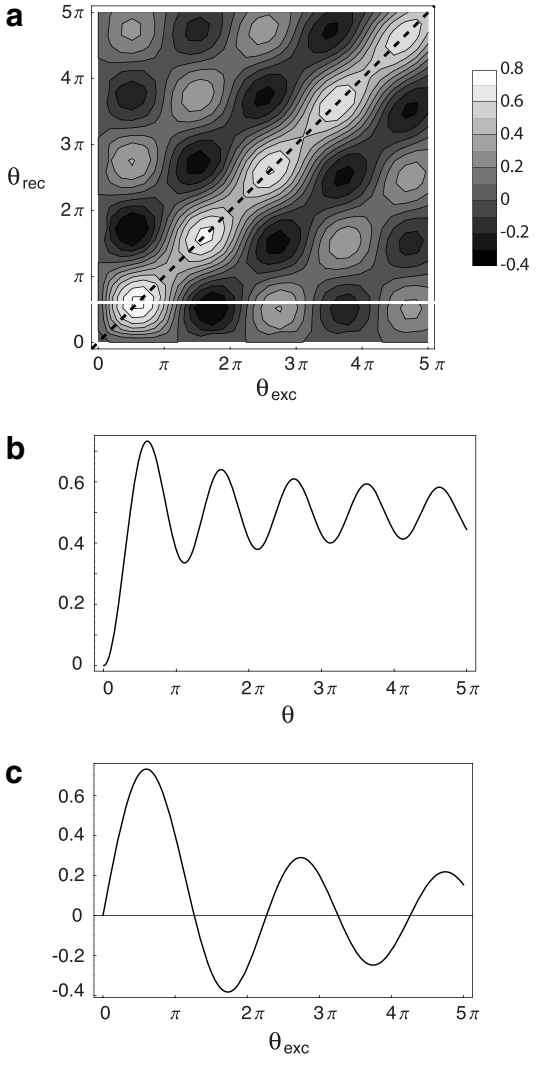

Fig. 2. (a) Contour plot of the universal DQF amplitude function $F_{\mathrm{DQ}}(\theta_{\mathrm{exc}}, \theta_{\mathrm{rec}})$ as a function of the angles θ_{exc} and θ_{rec}. (b) Symmetric DQF function $F_{\mathrm{DQ}}^{\mathrm{symm}}(\theta)$ as given in Eq. (36). This corresponds to a diagonal section through the contour plot in (a) (dashed line). (c) DQF amplitude function $F_{\mathrm{DQ}}(\theta_{\mathrm{exc}}, \theta_{\mathrm{rec}})$ as a function of θ_{exc}, with θ_{rec} fixed to the value $\theta_{\mathrm{rec}} = 0.602\pi$. This corresponds to a section through the contour plot in (a) along the white line. Note the large dynamic range in the oscillations.

4.1. Symmetric protocol

In the symmetric protocol [16], the intervals τ_{exc} and τ_{rec} are incremented simultaneously ($\tau_{\mathrm{exc}} = \tau_{\mathrm{rec}} = \tau$). The double-quantum-filtered signal amplitude is given by $F_{\mathrm{DQ}}^{\mathrm{symm}}(\theta) = F_{\mathrm{DQ}}(\theta, \theta)$ where

$$\theta = \tfrac{3}{2}|\kappa_{2m22}|b_{jk}\tau \tag{35}$$

In this case, the analytical solution simplifies to the following form:

$$F_{\mathrm{DQ}}^{\mathrm{symm}}(\theta) = \frac{1}{2} - \frac{1}{x\sqrt{8}}\Big(F_c(x\sqrt{2})\cos 2\theta + F_s(x\sqrt{2})\sin 2\theta\Big) \tag{36}$$

where

$$x = \left\{\frac{2\theta}{\pi}\right\}^{1/2} \tag{37}$$

A plot of Eq. (36) is shown in Fig. 2b, and displays the familiar oscillations with a maximum value of 73%, reached for a recoupling interval corresponding to $\theta = 0.602\pi = 108.3°$. The symmetric acquisition protocol corresponds to a diagonal section through the contour plot of $F_{\mathrm{DQ}}(\theta_{\mathrm{exc}}, \theta_{\mathrm{rec}})$, as shown by the dashed line in Fig. 2a.

4.2. Asymmetric protocol

In the asymmetric protocol [16], one of the two intervals τ_{exc} and τ_{rec} is kept fixed, while the other is incremented. The relevant modulation function may be expressed in universal form by using the angles θ_{exc} and θ_{rec}, as defined in Eq. (27). The asymmetric acquisition protocol corresponds to a section through a plot of $F_{\mathrm{DQ}}(\theta_{\mathrm{exc}}, \theta_{\mathrm{rec}})$, parallel to one of the axes. One such section is illustrated in Fig. 2c, which corresponds to the case where the angle θ_{exc} is varied, while θ_{rec} is fixed at the value 0.602π. This section corresponds to the white line in Fig. 2a and provides a particularly large dynamic range in the dipolar oscillations.

5. Numerical simulations

The analytical solutions were validated by comparisons with accurate numerical simulations of the spin dynamics using realistic parameters. The simulations shown in Figs. 3 and 4 used the spin system parameters defined in Table 1, which are typical for the ^{13}C-labelled retinals used in retinal protein studies. Unless stated otherwise, the simulated magnetic field strength was 9.4 T, and the simulated spinning frequency was 11.000 kHz. The simulated recoupling sequence had the symmetry $R20_2^9$, using the basic element $\mathcal{R}^0 = 90_0270_{180}$ [19]. All simulations used the symmetric incrementation protocol and were performed using SIMP-

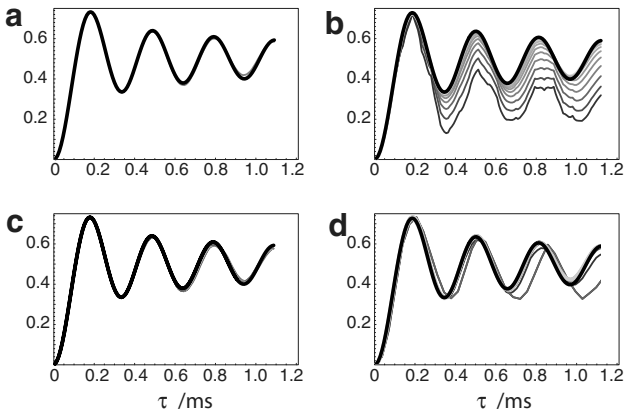

Fig. 3. Simulated curves for a typical $^{13}C_2$ spin system in the presence of $R20_2^9$ recoupling, using spin system parameters in Table 1, except when indicated. In all the plots the solid thick black line refers to the analytical curve $F_{DQ}^{symm}(\theta)$ in Eq. (36), where θ is defined in Eq. (35) and the scaling factor is $|\kappa_{2-122}| = 0.1743$. (a) Numerical simulations with both shift anisotropies set to zero (grey line); (b) numerical simulations with the shift anisotropy increased from 50 to 320 ppm/ for one site and from 30 to 300 ppm for the other site (the grey intensity increases with the increase in anisotropy); (c) numerical simulations obtained using 30 random values of the chemical shift tensor orientations (grey curves); (d) numerical simulations at different spinning frequencies in the range 3–21 kHz in steps of 3 kHz. The curve with the most visible deviation from the ideal is the 3 kHz curve.

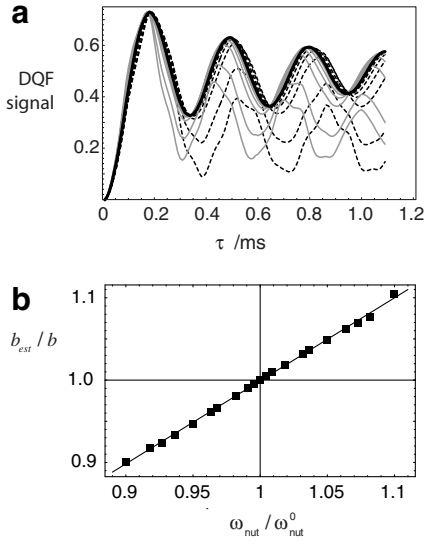

Fig. 4. (a) Dependence of the double-quantum-filtered signal on the excitation interval τ for the symmetric protocol using $R20_2^9$ recoupling. Numerical simulations using the parameters in Table 1 are shown for a set of nutation frequencies in the range 99–121 kHz. Rf amplitudes weaker and stronger than the nominal value of 110 kHz are shown as dashed lines and grey lines, respectively. The analytical solution is shown by a bold black curve; (b) ratio of the fitted dipolar coupling b_{est} to the true dipolar coupling b plotted against the ratio of the simulated rf nutation frequency to the nominal rf frequency. The straight line fit is also shown.

SON software [42]. The powder averages were calculated using 256 orientations, selected according to the REPULSION algorithm [43].

The solid black lines in all frames of Fig. 3 represent the symmetric analytical solution $F_{DQ}^{symm}(\theta)$ of Eq. (36), where the argument θ is related to the recoupling interval θ through Eq. (35). The dipole–dipole coupling constant b_{jk} is specified in Table 1. The scaling factor was calculated using the method of Brinkmann et al. [11] for the symmetry $R20_2^9$ and basic element $\mathcal{R}^0 = 90_0270_{180}$, and has the magnitude $|\kappa_{2-122}| = 0.1743$.

Fig. 3a compares the analytical solution (black) with a numerical simulation using the parameters given in Table 1, except for the chemical shift anisotropies, which were all set to zero (grey). The agreement is excellent in this idealized case.

In Fig. 3b, the analytical solution (black) is compared with a series of numerical simulations in which the chemical shift anisotropies are increased from 50 to 320 ppm for one site and from 30 to 300 ppm for the other, with the principal axis orientations fixed to the values specified in Table 1. Although the analytical and numerical results start to deviate at high chemical shift anisotropies, the positions of the maxima and minima do not vary significantly.

In Fig. 3c, the chemical shift principal values are fixed at the values in Table 1, but the principal axis orientations are randomized in a series of 30 simulations. The agreement between analytical and numerical results is good in all cases.

Fig. 3d explores the role of spinning frequency. Seven different simulations were performed for spinning frequencies $\omega_r/2\pi$ taking values $\{3.000, 6.000, 9.000, \ldots, 21.000\}$ kHz. In each case the rf nutation frequency was equal to 10 times the spinning frequency. The plots in Fig. 3d show little dependence on spinning frequency, except at the lowest spinning frequency, where the rf field is too small to dominate the chemical shift anisotropy.

Fig. 4a compares the analytical formula (black) with simulations at a fixed spinning frequency of 11.000 kHz, using a range of rf field nutation frequencies ω_{nut}, centred around the nominal nutation frequency of $\omega^0_{nut}/2\pi = 110.0$kHz. In this case there are noticeable deviations in the oscillation frequency of the curves as the rf field deviates from the nominal value. In order to assess the influence of rf field variations on the accuracy of the estimated dipolar coupling, we fitted each simulated curve in Fig. 4a to the analytical function $F_{DQ}^{symm}(\theta)$, allowing the dipolar coupling to vary. The estimated dipolar couplings $b_{est}(\omega_{nut})$ for each nutation frequency are plotted against the simulated nutation frequencies ω_{nut} in Fig. 4b. There is a linear dependence of the estimated dipolar coupling on the simulated nutation frequency, over the plotted range. A set of points with coordinates $(b_{est}b, \omega_{nut}\omega^0_{nut})$, where b is the true dipolar coupling, fall close to a straight line with a slope of 1.01. This indicates that a 1% error in the rf field value leads to a ~1% error in the dipolar coupling estimate, and hence a ~0.3% error in the estimate of the internuclear distance.

Table 1
Spin system parameters used in the numerical simulations

Parameter	Meaning	Value
$(\delta_j^{\mathrm{iso}}, \delta_k^{\mathrm{iso}})$	Isotropic chemical shifts	(−0.05 ppm, +0.05 ppm)
$(\delta_j^{\mathrm{aniso}}, \delta_k^{\mathrm{aniso}})$	Chemical shift anisotropies	(−101.5 ppm, 81.7 ppm)
(η_j, η_k)	Shift tensor biaxialities	(0.78,0.93)
J_{jk}	Isotropic J-coupling	0 Hz
$b_{jk}/2\pi$	Dipole–dipole coupling	−3.166 kHz
$(\alpha_{\mathrm{PM}}^{jk}, \beta_{\mathrm{PM}}^{jk}, \gamma_{\mathrm{PM}}^{jk})$	DD principal axis orientation	(0,0,0)
$(\alpha_{\mathrm{PM}}^{j}, \beta_{\mathrm{PM}}^{j}, \gamma_{\mathrm{PM}}^{j})$	CSA principal axis orientation	(−66.7°,77.3°,4.0°)
$(\alpha_{\mathrm{PM}}^{k}, \beta_{\mathrm{PM}}^{k}, \gamma_{\mathrm{PM}}^{k})$	CSA principal axis orientation	(−77.7°,11.0°, −9.1°)
B^0	Static magnetic field	9.39 T
$\omega_r/2\pi$	Spinning frequency	11.000 kHz
$\omega_{\mathrm{nut}}/2\pi$	Rf nutation frequency	110.0 kHz

The isotropic shifts are relative to the rf reference frequency. The Euler angles indicate the relative orientations of the tensor principal axis systems and a common molecular reference frame.

In summary, the numerical simulations given here show that the analytical formula may be used reliably to predict the double-quantum-filtered signal for $^{13}C_2$-labelled solids, even in the presence of rather large chemical shift anisotropies. However, a deviation in the rf field from the nominal value leads to a proportionate deviation in the estimated dipolar coupling from the true value.

6. Experimental results

A sample of [9,10-$^{13}C_2$]-*all-E*-retinal was obtained as a by-product in the synthesis of [9,10-$^{13}C_2$]-11*Z*-retinal [44]. The experiments described below were performed on a Varian Infinity + spectrometer, using 30 mg of 10% labeled [9,10-$^{13}C_2$]-*all-E*-retinal powder packed into a 4mm zirconium oxide rotor, spinning at 10.00 kHz in a magnetic field of 9.39 T (400 MHz proton Larmor frequency).

Longitudinal ^{13}C magnetization was generated by ramped cross-polarization [34] of duration 1.6 ms from the abundant ^1H nuclei, followed by a $\pi/2$ pulse with a $\pi/2$ phase shift. Double-quantum dipolar recoupling was accomplished using a sequence with the symmetry $R20_2^9$ based on the element $\mathcal{R}^0 = 90_0270_{180}$. The ^{13}C nutation frequency was 100.0 kHz during the recoupling sequences. Proton decoupling was not applied during the ^{13}C recoupling. A SPINAL-64 [45] proton decoupling sequence applied at 80 kHz was used during ^{13}C signal acquisition. In all cases, the double-quantum-filtered ^{13}C signal amplitudes were estimated by integrating the spectral peaks. These amplitudes were normalized against peak integrals from an equivalent cross-polarization experiment, without double-quantum filtration. The confidence limits on each experimental point were estimated by integrating several signal-free spectral regions of the same frequency bandwidth as that used for estimating the peak integrals. The standard deviation of these noise integrals were taken as the experimental confidence limits (shown by the error bars in Fig. 5).

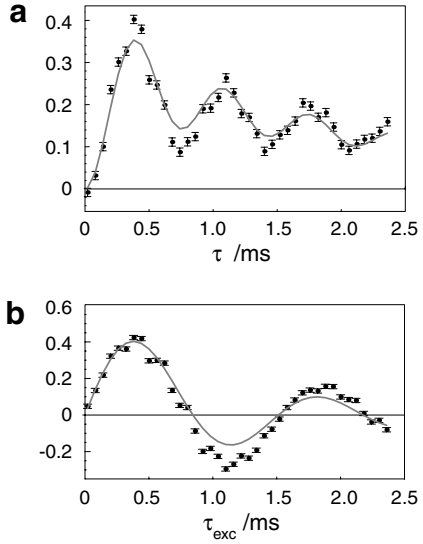

Fig. 5. Experimental double-quantum-filtered signal amplitudes for [9,10-$^{13}C_2$]-*all-E*-retinal obtained using the $R20_2^9$ pulse sequence at a spinning frequency of $\omega_r/2\pi = 11.00$ kHz. (a) Symmetric acquisition protocol, with both recoupling intervals varied, $\tau = \tau_{\mathrm{exc}} = \tau_{\mathrm{rec}}$. The solid grey curve is the best fit to Eq. (38). (b) Asymmetric acquisition protocol, with τ_{rec} fixed at 400 μs and τ_{exc} varied. The solid grey curve is the best fit to Eq. (39).

Fig. 5a shows experimental double-quantum-filtered signal amplitudes for the symmetric protocol, with τ_{exc} and τ_{rec} incremented simultaneously from 0 to 2.36 ms in steps of 60 μs. The maximum double-quantum filtering efficiency was about 40%. The grey line in Fig. 5a shows the best fit of the function

$$A F_{\mathrm{DQ}}^{\mathrm{symm}}(\theta) \exp\{-2\tau/T_{\mathrm{decay}}\} \tag{38}$$

where θ depends on the dipolar coupling and τ according to Eq. (35), the function $F_{\mathrm{DQ}}^{\mathrm{symm}}$ is given by Eq. (36), the scaling factor $|\kappa_{2-122}|$ is fixed to the value 0.1743, and b_{jk} and T_{decay} are fit parameters. The best fit curve has the parameters $|b_{jk}/2\pi| = 2.845$ kHz, $A = 0.56$ and $T_{\mathrm{decay}} = 1.88$ ms.

The low value of A reflects an unexplained overall loss in the double-quantum-filtered signal. This is a common observation when performing recoupling experiments at moderately high spinning frequencies, and is tentatively attributed to imperfect heteronuclear decoupling and radiofrequency imperfections.

Fig. 5b shows experimental results for the asymmetric protocol, with τ_{rec} fixed at 400 μs. The grey line in Fig. 5b shows the best fit of the function

$$AF_{\mathrm{DQ}}(\theta_{\mathrm{exc}}, \theta_{\mathrm{rec}}) \exp\left\{-(\tau_{exc} + \tau_{rec})/T_{\mathrm{decay}}\right\} \quad (39)$$

where T_{decay} was fixed at 1.88 ms and F_{DQ} is given by Eq. (30). The angles $\{\theta_{\mathrm{exc}}, \theta_{\mathrm{rec}}\}$ depend on the dipolar coupling and the intervals $\{\tau_{exc}, \tau_{rec}\}$ according to Eq. (27). The best fit curve has the parameters $|b_{jk}/2\pi| = 2.863$ kHz and $A = 0.63$.

The analytical curves fit the experimental data quite well, although the experimental data displays somewhat larger dipolar oscillations compared to theoretical expectations. This phenomenon is not fully understood but may be associated with anisotropy in the cross-polarization.

The confidence limits on the determined dipolar coupling are determined by the noise on the experimental signal amplitudes and the uncertainty in the applied rf nutation frequency. The rf error term dominates in this case. We estimate the uncertainty in the nutation frequency to be around ±3%. From Fig. 4, the estimated value of the dipole–dipole coupling is also subject to ~3% uncertainty. The estimated dipole–dipole coupling is therefore $b_{jk}/2\pi = -2.85 \pm 0.09$ kHz.

If motion and J-anisotropy is neglected, the dipolar coupling may be converted into an estimated internuclear distance. In the present case, this leads to an internuclear distance estimate of 138 ± 1 pm. The X-ray crystallographic estimate for the same substance is 134.5 pm [46]. The discrepancy between the NMR and X-ray estimates of the internuclear distance in this compound is therefore 3.5 ± 1 pm, with the NMR distance estimate being the larger one. This small discrepancy in the distance estimates for the two techniques is typical for ^{13}C–^{13}C internuclear distances in organic compounds [16].

7. Conclusions

We have derived closed analytical solutions for the powder-average signal amplitudes involved in γ-encoded double-quantum recoupling experiments. These solutions may be evaluated much more rapidly than explicit spin dynamical calculations, which greatly facilitates the determination of dipole–dipole coupling constants from experimental data. The analytical formulae were applied to a dipole coupling estimation for the $^{13}C_2$ spin pairs in [9,10-$^{13}C_2$]-*all*-*E*-retinal. The dipolar coupling estimate corresponds to an internuclear distance which is within 4 pm of the X-ray value.

Similar analytical expressions may be derived for other γ-encoded recoupling problems, such as magnetization transfer curves under rotational resonance [25,26], and sideband-matched Hartmann–Hahn cross-polarization [47–49]. Even the Hamiltonian of isolated spin pairs in *static* solids has a γ-encoded form, due to the rotational symmetry around the static magnetic field. The analytical form of the free-induction decay in static powders containing isolated spin-1/2 pairs also involves Fresnel functions [41].

A word of caution: each technique has its own sensitivity to interference from extraneous spin interactions, and to experimental imperfections. The analytical formulae should therefore never be applied blindly without performing test simulations in the regime of interest.

Acknowledgments

This research was supported by the EPSRC (UK). We thank Ole G. Johannessen for experimental support, Marina Carravetta for discussions, and Giulia Mollica for bringing previous NMR applications of Fresnel integrals [41] to our attention.

References

[1] E.R. Andrew, A. Bradbury, R.G. Eades, Removal of dipolar broadening of nuclear magnetic resonance spectra of solids by specimen rotation, Nature 183 (1959) 1802.
[2] I.J. Lowe, Free induction decays of rotating solids, Phys. Rev. Lett. 2 (1959) 285.
[3] A. Pines, M.G. Gibby, J.S. Waugh, Proton-enhanced nuclear induction spectroscopy. A method for high resolution NMR of dilute spins in solids, J. Chem. Phys. 56 (1972) 1776.
[4] A. Pines, M.G. Gibby, J.S. Waugh, Proton-enhanced NMR of dilute spins in solids, J. Chem. Phys. 59 (1973) 569.
[5] R. Tycko, G. Dabbagh, Measurement of dipole–dipole couplings in magic angle spinning NMR, Chem. Phys. Lett. 173 (1990) 461.
[6] N.C. Nielsen, H. Bildsøe, H.J. Jakobsen, M.H. Levitt, Double-quantum homonuclear rotary resonance: efficient dipolar recovery in magic-angle-spinning nuclear magnetic resonance, J. Chem. Phys. 101 (1994) 1805.
[7] Y.K. Lee, N.D. Kurur, M. Helmle, O.G. Johannessen, N.C. Nielsen, M.H. Levitt, Efficient dipolar recoupling in the NMR of rotating solids: a seven-fold symmetric radiofrequency pulse sequence, Chem. Phys. Lett. 242 (1995) 304–309.
[8] M. Hohwy, H.J. Jakobsen, M. Edén, M.H. Levitt, N.C. Nielsen, Broadband dipolar recoupling in the NMR of rotating solids. A compensated C7 pulse sequence, J. Chem. Phys. 108 (1998) 2686.
[9] A. Brinkmann, M. Edén, M.H. Levitt, Synchronous helical pulse sequences in magic-angle spinning NMR. Double quantum recoupling of multiple-spin systems, J. Chem. Phys. 112 (2000) 8539–8554.
[10] M. Edén, M.H. Levitt, Pulse sequence symmetries in the NMR of spinning solids. Application to heteronuclear decoupling, J. Chem. Phys. 111 (1999) 1511–1519.
[11] A. Brinkmann, M.H. Levitt, Symmetry principles in the nuclear magnetic resonance of spinning solids: heteronuclear recoupling by generalized Hartmann-Hahn sequences, J. Chem. Phys. 115 (2001) 357–384.
[12] C.E. Hughes, S. Luca, M. Baldus, Radio-frequency driven polarization transfer without heteronuclear decoupling in rotating solids, Chem. Phys. Lett. 385 (2004) 435–440.
[13] I. Marin-Montesinos, G. Mollica, M. Carravetta, A. Gansmüller, G. Pileio, M. Bechmann, A. Sebald, M.H. Levitt, Truncated dipolar

recoupling in solid-state nuclear magnetic resonance, Chem. Phys. Lett. 432 (2006) 572–578.
[14] M. Carravetta, M. Edén, X. Zhao, A. Brinkmann, M.H. Levitt, Symmetry principles for the design of radiofrequency pulse sequences in the nuclear magnetic resonance of rotating solids, Chem. Phys. Lett. 321 (2000) 205–215.
[15] A. Brinkmann, J. Schmedt auf der Günne, M.H. Levitt, Homonuclear zero-quantum recoupling in fast magic-angle spinning nuclear magnetic resonance, J. Magn. Reson. 56 (2002) 79–96.
[16] M. Carravetta, M. Edén, O.G. Johannessen, H. Luthman, P.J.E. Verdegem, J. Lugtenburg, A. Sebald, M.H. Levitt, Estimation of carbon–carbon bond lengths and medium-range internuclear distances by solid-state nuclear magnetic resonance, J. Am. Chem. Soc. 123 (2001) 10628–10638.
[17] P.E. Kristiansen, M. Carravetta, W.C. Lai, M.H. Levitt, A robust pulse sequence for the determination of small homonuclear dipolar couplings in magic-angle spinning NMR, Chem. Phys. Lett. 390 (2004) 1–7.
[18] P.E. Kristiansen, M. Carravetta, J.D. van Beek, W.C. Lai, M.H. Levitt, Theory and applications of supercycled symmetry-based recoupling sequences in solid-state NMR, J. Chem. Phys. 124 (2006) 234510–234519.
[19] I. Marin-Montesinos, D.H. Brouwer, G.C. Antonioli, W.C. Lai, A. Brinkmann, M.H. Levitt, Heteronuclear decoupling interference during symmetry-based homonuclear recoupling in solid-state NMR, J. Magn. Reson. 177 (2005) 307–317.
[20] M.H. Levitt, Symmetry-based pulse sequences in magic-angle spinning solid-state NMR, in: D.M. Grant, R.K. Harris (Eds.), Encyclopedia of Nuclear Magnetic Resonance: Supplementary Volume, Wiley, Chichester, UK, 2002.
[21] S.-F. Liu, J.D. Mao, K. Schmidt-Rohr, A robust technique for two-dimensional separation of undistorted chemical-shift anisotropy powder patterns in magic-angle-spinning NMR, J. Magn. Reson. 155 (2002) 15–28.
[22] M. Bak, N.C. Nielsen, Relative orientation of chemical shielding and dipolar coupling tensors: Mixed single-and double-quantum homonuclear rotary resonance NMR of rotating solids, J. Chem. Phys. 106 (1997) 7587.
[23] T. Gullion, J. Schaefer, Rotational-echo double-resonance NMR, J. Magn. Reson. 81 (1989) 196–200.
[24] T. Gullion, J. Schaefer, Detection of weak heteronuclear couplings by REDOR, Adv. Magn. Reson. 13 (1989) 57.
[25] D.P. Raleigh, M.H. Levitt, R.G. Griffin, Rotational resonance in solid-state NMR, Chem. Phys. Lett. 146 (1988) 71.
[26] M.H. Levitt, D.P. Raleigh, F. Creuzet, R.G. Griffin, Theory and simulations of homonuclear spin-pair systems in rotating solids, J. Chem. Phys. 92 (1990) 6347–6364.
[27] A.W. Hing, S. Vega, J. Schaefer, Transfer-echo double-resonance NMR, J. Magn. Reson. 96 (1992) 205.
[28] A.E. Bennett, J.H. Ok, R.G. Griffin, S. Vega, Chemical shift correlation spectroscopy in rotating solids: Radio frequency-driven dipolar recoupling and longitudinal exchange, J. Chem. Phys. 96 (1992) 8624.
[29] K.T. Mueller, Analytic solutions for the time evolution of dipolar-dephasing NMR signals, J. Magn. Reson. 113 (1995) 81–93.
[30] K.T. Mueller, T.P. Jarvie, D.J. Aurentz, B.W. Roberts, The REDOR transform: direct calculation of internuclear couplings from dipolar-dephasing NMR data, Chem. Phys. Lett. 242 (1995) 535–542.
[31] K.T. Mueller, T.P. Jarvie, D.J. Aurentz, B.W. Roberts, Erratum and comment on ''The REDOR transform: direct calculation of internuclear couplings from dipolar-dephasing NMR data'', Chem. Phys. Lett. 254 (1995) 281–282.
[32] D.H. Brouwer, P.E. Kristiansen, C.A. Fyfe, M.H. Levitt, Symmetry-Based ^{29}Si dipolar recoupling magic angle spinning NMR spectroscopy: a new method for investigating three-dimensional structures of zeolite frameworks, J. Am. Chem. Soc. 127 (2005) 542–543.
[33] D.H. Brouwer, R.J. Darton, R.E. Morris, M.H. Levitt, A solid-state NMR method for the solution of zeolite crystal structures, J. Am. Chem. Soc. 127 (2005) 10365–10370.
[34] G. Metz, X. Wu, S.O. Smith, Ramped-amplitude cross polarization in magic-angle-spinning NMR, J. Magn. Reson. A 110 (1994) 219.
[35] R.R. Ernst, G. Bodenhausen, A. Wokaun, Principles of Nuclear Magnetic Resonance in One and Two Dimensions, Clarendon Press, Oxford, 1987.
[36] U. Haeberlen, J.S. Waugh, Coherent averaging effects in magnetic resonance, Phys. Rev. 175 (1968) 453–467.
[37] J. Jeener, Superoperators in magnetic resonance, Adv. Magn. Reson. 10 (1982) 1.
[38] G.N. Watson, Theory of Bessel Functions, Cambridge University Press, Cambridge, 1944.
[39] M. Abramowitz, I.A. Stegun, Handbook of Mathematical Functions, Dover, New York, 1965.
[40] S. Wolfram, Mathematica: A System for Doing Mathematics by Computer, Addison-Wesley, New York, 1991.
[41] D.C. Look, I.J. Lowe, J.A. Northby, Nuclear magnetic resonance study of molecular motions in solid hydrogen sulfide, J. Chem. Phys. 44 (1966) 3441–3452.
[42] M. Bak, J.T. Rasmussen, N.C. Nielsen, SIMPSON: A general simulation program for solid-state NMR spectroscopy, J. Magn. Reson. 147 (2000) 296–330.
[43] M. Bak, N.C. Nielsen, REPULSION, A novel approach to efficient powder averaging in solid-state NMR, J. Magn. Reson. 125 (1997) 132.
[44] The $^{13}C_2$-retinals were prepared from acetic acid-1-^{13}C and triethyl phosphonoacetate-2-^{13}C in 13 steps. The stereocontrolled synthesis of doubly-labeled retinal isotopomers will be reported elsewhere.
[45] B.M. Fung, A.K. Khitrin, K. Ermolaev, An Improved broadband decoupling sequence for liquid crystals, J. Magn. Reson. 142 (2000) 97–101.
[46] T. Hamanaka, T. Mitsui, T. Ashida, M. Kakudo, The crystal structure of all-trans retinal, Acta Cryst. B. 28 (1972) 214.
[47] E.O. Stejskal, J. Schaefer, J.S. Waugh, Magic-angle spinning and polarization transfer in proton-enhanced NMR, J. Magn. Reson. 28 (1977) 105.
[48] B.-J. van Rossum, C.P. de Groot, V. Ladizhansky, S. Vega, H.J.M. de Groot, A method for measuring heteronuclear (^{1}H-^{13}C) distances in high speed MAS NMR, J. Am. Chem. Soc. 122 (2000) 3465–3472.
[49] M. Baldus, A.T. Petkova, J. Herzfeld, R.G. Griffin, Cross polarization in the tilted frame: assignment and spectral simplification in heteronuclear spin systems, Mol. Phys. 95 (1998) 1197.